jmb Communication

Structural Basis for the ATP-Induced Isomerization of Kinesin

Qing Chang[1,2], Ryo Nitta[1,2], Shigeyuki Inoue[1,2] and Nobutaka Hirokawa[1,2,3]

*1 - **Department of Cell Biology and Anatomy,** Graduate School of Medicine, The University of Tokyo, Hongo, Tokyo 113-0033, Japan*
*2 - **Department of Molecular Structure and Dynamics,** Graduate School of Medicine, The University of Tokyo, Hongo, Tokyo 113-0033, Japan*
*3 - **Center of Excellence in Genomic Medicine Research (CEGMR),** King Abdulaziz University, Jeddah 21589, Saudi Arabia*

***Correspondence to Nobutaka Hirokawa:** Department of Cell Biology and Anatomy, Graduate School of Medicine, The University of Tokyo, Hongo, Tokyo 113-0033, Japan. hirokawa@m.u-tokyo.ac.jp*
http://dx.doi.org/10.1016/j.jmb.2013.03.004
Edited by G. Schulz

Abstract

Kinesin superfamily proteins (KIFs) are microtubule-based molecular motors driven by the energy derived from the hydrolysis of ATP. Previous studies have revealed that the ATP binding step is crucial both for the power stroke to produce motility and for the inter-domain regulation of ATPase activity to guarantee the processive movement of dimeric KIFs. Here, we report the first crystal structure of KIF4 complexed with the non-hydrolyzable ATP analog, AMPPNP (adenylyl imidodiphosphate), at 1.7 Å resolution. By combining our structure with previously solved KIF1A structures complexed with two ATP analogs, molecular snapshots during ATP binding reveal that the closure of the nucleotide-binding pocket during ATP binding is achieved by closure of the backdoor. Closure of the backdoor stabilizes two mobile regions, switch I and switch II, to generate the phosphate tube from which hydrolyzed phosphate is released. Through the stabilization of switch II, the local conformational change at the catalytic center is further relayed to the neck-linker element that fully docks to the catalytic core to produce the power stroke. Because the neck linker is a sole element that connects the partner heads in dimeric KIFs, this tight structural coordination between the catalytic center and neck linker enables inter-domain communication between the partner heads. This study also revealed the putative microtubule-binding site of KIF4, thus providing structural insights that describe the specific binding of KIF4 to the microtubule.

Kinesin superfamily proteins (KIFs) are molecular motors that play crucial roles in the intracellular transport of membranous organelles, protein complexes, and mRNAs along microtubules.[1] The energy required for KIF motility is supplied by ATPase cycling. ATP is catalyzed in the catalytic center (nucleotide-binding pocket) of the kinesin motor domain and the liberated energy is conveyed to the microtubule-binding surface distal from the catalytic center to produce movement or mechanical work.[2,3]

For dimeric KIFs, which are thought to be driven by the asymmetric hand-over-hand mechanism,[4,5] the binding of ATP to the catalytic core represents the crucial step for microtubule-based motility. This is because this step not only produces the power stroke that brings the tethered head to the next binding site[6] but also regulates the ATPase activity of the partner head to guarantee the processivity of dimeric motility (ATP gating).[7,8] To elucidate the structural basis for ATP binding, we first solved the crystal structure of kinesin in the ATP state for KIF1A complexed with the non-hydrolyzable ATP analog, AMPPCP (β,γ-methyleneadenosine 5-triphosphate),[9] immediately followed by KIF1A complexed with the non-hydrolyzable ATP analog, AMPPNP (adenylyl imidodiphosphate).[10] Subsequently, the AMPPNP states for the non-motile kinesin, NOD, and the mitotic kinesin, Eg5, were also reported, which assume a different conformation around the nucleotide-binding pocket compared to KIF1A.[11,12] In parallel, cryo-electron microscopy (cryo-EM) structures of KIFs-AMPPNP complexed with microtubules at resolutions of ≈10 Å were solved for KIF1A, KIF5, and kar3.[13–15]

These structures revealed that conformational changes in the neck linker serve as a conduit to connect both heads (motor domains) in dimeric KIFs and contribute to both the power stroke and the regulation of the ATPase. However, discrepancies have been reported between the crystal and cryo-EM structures, and these differences are primarily concentrated in the switch I and switch II regions, which change their conformations during the ATPase cycle.[13,15] Although Sindelar and Downing reported in a footnote that the crystal structure of Eg5 and the cryo-EM structure of KIF5 assume similar conformations,[15] these observations are still under debate because KIF1A, KIF5, and kar3 apparently assume different conformations in the same nucleotide states.[8,10,14,15]

Here, we report the first crystal structure of KIF4 complexed with the non-hydrolyzable ATP analog, AMPPNP. The high-resolution structure of the KIF4 motor domain revealed that the ATP state of the motor domain fitted perfectly into the cryo-EM structure of the KIF5–microtubule complex, even for the structural elements around the nucleotide-binding pocket.[15] More importantly, in comparison with previously solved structures of the KIF1A, KIF5, and Eg5 motor domains, N-kinesins including KIF1A, KIF4, KIF5, and Eg5 utilize the same strategy for the nucleotide-induced conformational change. By combining structural data for KIF4 and KIF1A, the atomic detail of the local conformational change at the catalytic center induced by ATP binding, and how this local change is relayed to the microtubule-binding surface that is distal from the catalytic center, were determined. This study also provides structural insights that describe how KIF4 specifically binds to the microtubule.

Overall architecture of the KIF4 motor domain

The x-ray crystal structure of the motor domain of KIF4 with AMPPNP was refined to values of 1.7 Å (Table S1). The motor domain has a similar architecture to previously solved motor domains of several KIFs (Fig. 1a and Table S2). KIF4 has a layer of central β-sheets that is sandwiched between two layers of α-helices (Fig. 1b). The N-terminal half of the catalytic core forms both the top α-helix layer and the central β-sheet layer and contains the ATPase reaction center. The phosphate-binding loop, L4, namely, the "P-loop", forms a shallow groove (the nucleotide-binding pocket) on the top surface of the catalytic core in which ATP is trapped. The C-terminal half of the helix, α3, and the following loop, L9, namely, switch I, are also located in close proximity to the catalytic center and contribute to the effective hydrolysis of ATP.[8,10] The C-terminal half of the catalytic core forms the bottom α-helix layer that contains a series of five structural elements: loop L11, helix α4, loop L12, helix α5, and loop L13. This region is known as switch II owing to its analogy to the switch II structural element in G proteins, and it serves as the binding surface for the microtubule (Fig. 1b).[21]

To identify the conformational differences between KIF4–AMPPNP and the previously solved motor domain structures of other N-kinesins complexed with AMPPNP, we superimposed the KIF4–AMPPNP structure with the previously solved

Fig. 1. Overall architecture of the KIF4 motor domain. (a) The KIF4 motor domain seen from the microtubule binding side. The P-loop, switch I, switch II, and neck linker are shown in yellow, red, green, and orange, respectively. (b) The KIF4 motor domain seen from the right side. Color coding is the same as (a). (c–f) Superposition of KIF4–AMPPNP (red) and KIF1A–AMPPNP (blue) (c and d) and of KIF4–AMPPNP (red) and Eg5–AMPPNP (green) (e and f) from the microtubule-binding side (c and e) and from the opposite side (d and f). A KIF4 motor domain construct, KIF4-344 [residues 1–344 of KIF4 followed by a $(His)_7$ tag], was cloned into the pET21b vector (Novagen) and transformed into BL21(DE3) cells (Novagen) for expression. Cells were grown in YT media with 0.5% glycerol, 0.05% glucose, and 0.2% β-lactose at 30 °C for 10 h; resuspended in lysis buffer (50 mM Tris–HCl, pH 8.0, 150 mM NaCl, 5% glycerol, 5 mM imidazole, and protease inhibitors); and lysed using a French press (Ohtake). The soluble protein fraction was loaded onto a His-select nickel affinity column (Sigma) equilibrated with the lysis buffer, and 500 mM imidazole was used to elute the bound protein. The pooled fractions were dialyzed against CIEX buffer (50 mM Hepes, pH 7.0, and 50 mM NaCl), loaded onto a RESOURCE S column (GE Healthcare) equilibrated with CIEX buffer, and a linear gradient of NaCl was applied to elute the protein. The pooled protein fractions were then dialyzed against SEC buffer (10 mM Tris–HCl, pH 8.0, 500 mM NaCl, and 1 mM DTT) and loaded onto a Superdex 200 10/300 GL column (GE Healthcare) equilibrated with SEC buffer. The final protein fractions were dialyzed against the final buffer (10 mM Tris–HCl, pH 8.0, 100 mM NaCl, and 1 mM DTT), concentrated to 15 mg ml^{-1}, and used for crystallization with the vapor diffusion method (sitting drop). Crystals of KIF4–AMPPNP were obtained using the reservoir buffer (28% w/v polyethylene glycol 4000, 100 mM Tris–HCl, pH 8.5, and 200 mM sodium acetate) in the presence of 5 mM AMPPNP. X-ray diffraction data of KIF4–AMPPNP were collected at −180 °C to 1.71 Å on the beam line BL41XU (wavelength λ = 1.00 Å) at SPring8 and to 1.80 Å on the beam line NW12A (wavelength λ = 1.00 Å) at the Photon Factory (PF). All data were integrated using XDS[16] and scaled using Pointless and Scala[17] (see Table S1 for the data collection statistics). The structures of KIF4–AMPPNP were determined by molecular replacement with MOLREP[18] using the Eg5 structure (3HQD) as a starting model. After subsequent rounds of model building and refinement using Refmac5[19] and Coot,[20] the electron density maps were improved, resulting in R and R_{free} values of 15.6% and 18.8% for KIF4–AMPPNP at SPring8 and 16.4% and 19.7% for KIF4–AMPPNP at the PF, respectively (see Table S1 for the refinement statistics).

KIF1A–AMPPNP and Eg5–AMPPNP structures (Fig. 1c–f) (Protein Data Bank ID: 1VFV for KIF1A and 3HQD for Eg5).[10,12] Although the overall architecture of KIF4–AMPPNP is similar to the previously solved KIF1A and Eg5 structures (Table S2), several differences were found between KIF4 and KIF1A, between KIF4 and Eg5, or between all of these motors. These conformational differences can

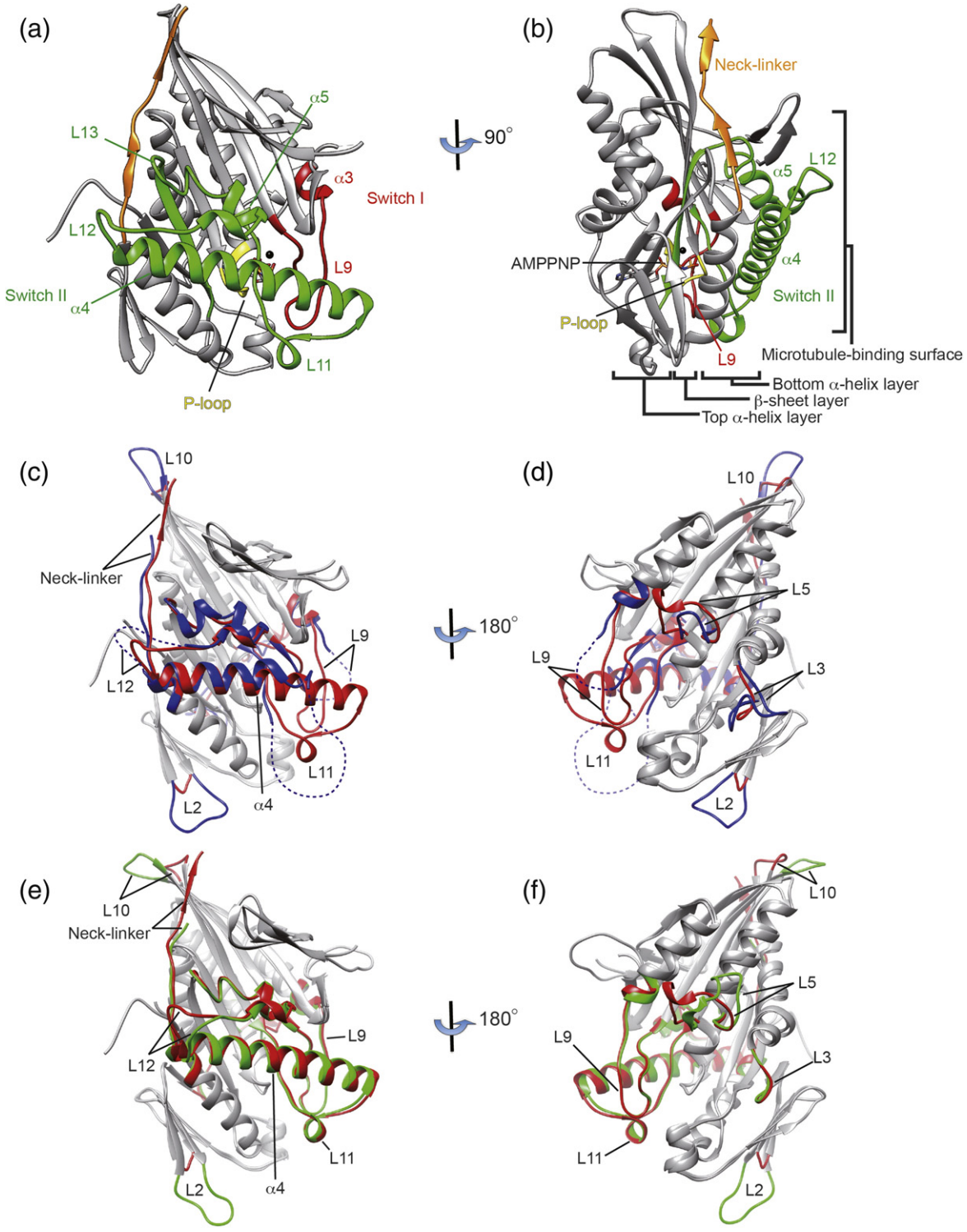

Fig. 1 (*legend on previous page*)

be conceptually divided into two types: class-specific differences independent from the nucleotide-induced conformational change and nucleotide-induced conformational differences observed at switch I, switch II, and the neck linker (Fig. 1c–f).

The class-specific conformational differences are basically observed in the loop regions located in the top α-helix layer or in the central β-sheet layer. Several variations in the amino acid sequences or the lengths of loops are observed, particularly in loops L3 and L5 in the top α-helix layer and in loops L2 and L10 in the central β-sheet layer. Eg5 has the longest loop L5 of 19 residues, whereas KIF1A has the shortest loop L5 of 10 residues. KIF1A has an 8-residue insertion at loop L3. KIF4 has the shortest loops L2 and L10, such that KIF4 is apparently a short-nosed and short-tailed motor. Here, it might be meaningful that these loops are accessible from the outside of the motor domain even in KIFs attaching to the microtubule. For example, loop L5 is located at the other side of the microtubule-binding surface and just above the nucleotide-binding pocket such that modification or conformational change of L5 induced from the outside should affect the ATPase activity of the motor domains. These loops are, therefore, possible candidates for the class-specific regulation of KIF motility from the outside of the motor domain.

In contrast, the nucleotide-induced conformational differences are mainly observed at the microtubule-binding side of the bottom α-helix layer (switch II and neck linker) and the linkage (switch I) between the nucleotide-binding pocket and the microtubule-binding surface. These regions are highly conserved between N-kinesins and are tightly related to general ATPase cycling, and N-kinesins have an apparently conserved structural mechanism of ATP hydrolysis. These regions in the same nucleotide state, therefore, should assume the same conformation in different N-kinesins. As detailed below, KIF4 and Eg5 assume a similar conformation for the two switch regions and the neck linker, but KIF1A does not, particularly for switch I (Table S2).

In the switch I region, loop L9 is disordered in the KIF1A–AMPPNP complex (blue in Fig. 1c and d), whereas it is well ordered and comes closer to the nucleotide-binding pocket in both the KIF4–AMPPNP complex (average *B*-factor for L9 of KIF4, 9.8 $Å^2$) (red in Fig. 1c–f) and the Eg5–AMPPNP complex (green in Fig. 1c–f). In the switch II region, loop L11 is mostly disordered in KIF1A–AMPPNP (blue in Fig. 1c and d), whereas it is well ordered and the loop-to-helix transition is observed in both the KIF4–AMPPNP (average *B*-factor for L11 of KIF4, 18.2 $Å^2$) (red in Fig. 1c–f) and Eg5–AMPPNP complexes (green in Fig. 1c–f). The neck linker binds to the catalytic core more tightly in KIF4 and Eg5 than KIF1A, and these interactions are mainly mediated by main-chain residues, such as the arrangement seen in the β-sheet (Fig. 1c–f). Hence, we will discuss in the following section how these conformational differences can be structurally explained by the high-resolution structures of the KIF4 and KIF1A motor domains. It should be noted that both the KIF4 and KIF1A structures complexed with AMPPNP were solved at very high resolution (<1.8 Å) with high-quality refinement (Table S1) and therefore we can firmly discuss their differences below with respect to not only the interactions between side chains but also the water-mediated hydrogen-bond network.

Kinesin is a backdoor enzyme

The motor domains of KIFs complexed with AMPPNP are expected to represent the ATP state, that is, the state just prior to ATP hydrolysis (pre-hydrolysis state). By analogy with myosin, which is thought to have the same ancestral molecule as KIFs,[22] the following two features are necessary for the pre-hydrolysis conformation.[23] (1) Both the conserved serine 211 (SSRSH) in the switch I region and glycine 244 (DLAGSE) in the switch II region directly interact with the γ-phosphate, serving as the γ-phosphate sensor to trigger ATP hydrolysis and the subsequent large conformational changes in switch II ("relay helix" in myosins). (2) The salt bridge between the conserved arginine 212 (SSRSH) in switch I and glutamate 246 (DLAGSE) in switch II, which is called the "backdoor", is formed to close the nucleotide-binding pocket.

In the electron density map of the KIF4 motor domain, the AMPPNP moiety is clearly observed in the nucleotide-binding pocket (Fig. 2c). The KIF4–AMPPNP structure possesses both features necessary for the pre-hydrolysis state. The γ-phosphate of AMPPNP tightly interacts with both S211 in switch I

Fig. 2. Isomerization reaction around the catalytic center during ATP binding. (a) Catalytic center at the pre-isomerization state with KIF1A–AMPPCP. The conserved serine and glycine residues are still away from the γ-phosphate of AMPPCP. (b) Catalytic center at the isomerization intermediate state with KIF1A–AMPPNP. The γ-phosphate is sensed by the conserved residues with one catalytic water (W1) trapped. The backdoor is partially closed. (c) Catalytic center at the pre-hydrolysis state with KIF4–AMPPNP. The γ-phosphate is sensed by the conserved residues and the backdoor is completely closed, trapping the two catalytic waters (W1 and W2) in the pocket. (d and e) Phosphate tube seen in the KIF4–AMPPNP structure. Ribbon model together with the theoretical 8-Å map calculated from the atomic model is shown. The γ-phosphate and backdoor are located at the entrance and the exit of the phosphate tube, respectively. (e) The view from the exit of the phosphate tube (blue). (f) Stabilization of switch I and switch II by several key interactions.

and G244 in switch II (Fig. 2c). The backdoor salt bridge is also tightly formed. In the KIF1A–AMPPNP structure, however, the latter feature is partially formed (Fig. 2b). The corresponding serine and glycine residues come closer to the γ-phosphate within the hydrogen-bond ranges. The backdoor salt

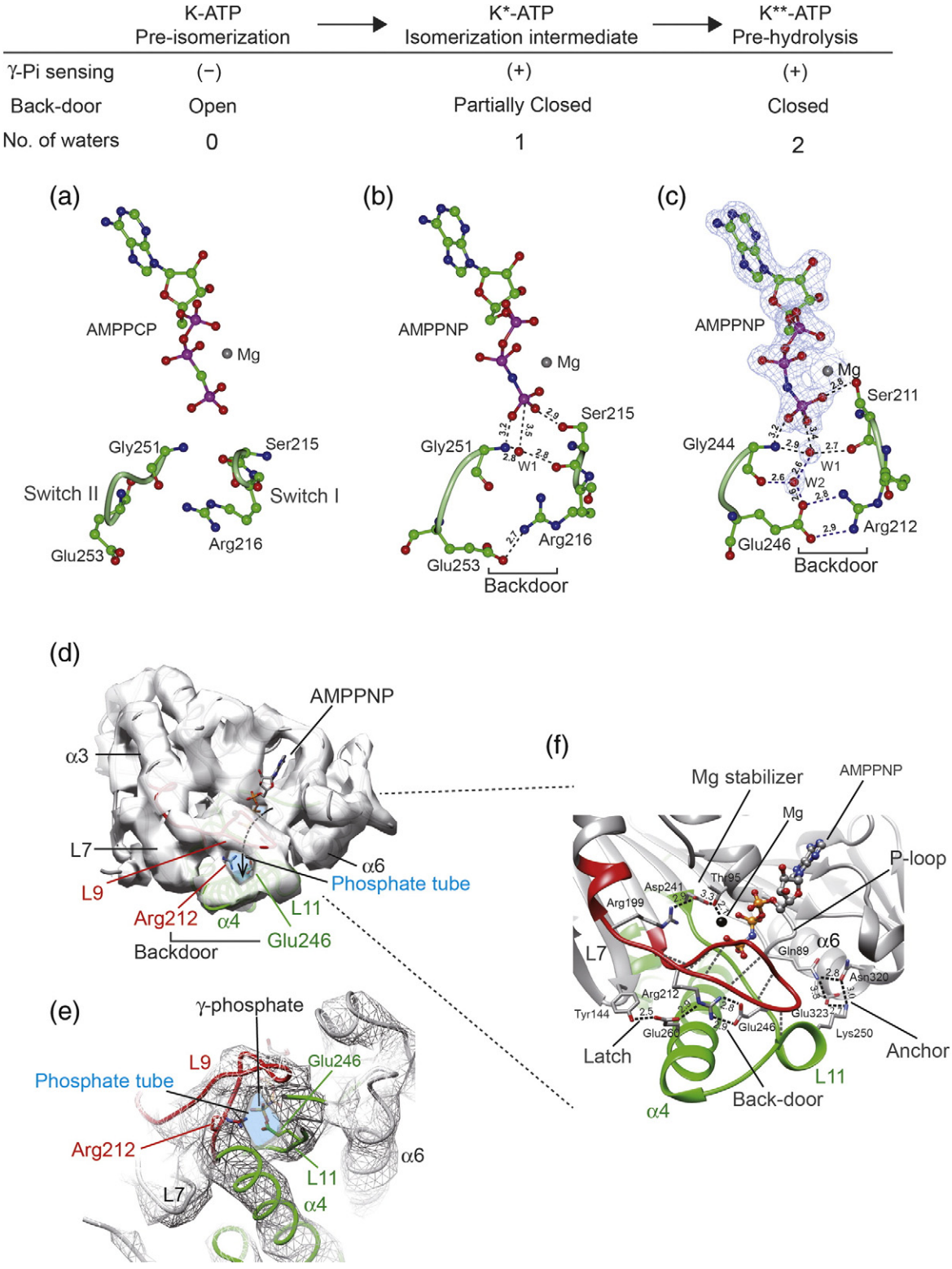

Fig. 2 (*legend on previous page*)

bridge, however, is partially closed with only one ionic interaction found. The structure of the ATP state of KIF1A was also solved with another non-hydrolyzable ATP analog, AMPPCP.[9] In this structure, the γ-phosphate of AMPPCP in KIF1A is distant from the γ-phosphate-sensing residues and the backdoor residues are far from each other (open) such that the conformation lacks both features required for the formation of the pre-hydrolysis state (Fig. 2a).

These conformational changes around the γ-phosphate allow water molecules to be sequentially recruited to the nucleotide-binding pocket for nucleophilic attack of the γ-phosphorus. In the KIF1A–AMPPCP structure, no water molecules were found within the hydrogen-bonding range from the γ-phosphate (Fig. 2a). In the KIF1A–AMPPNP structure, the highly conserved Ser (switch I) and Gly (switch II) residues recruit one water molecule into the nucleotide-binding pocket and serve it to the γ-phosphate (Fig. 2b). In the KIF4–AMPPNP structure, the backdoor further recruits another water molecule next to the first water molecule, such that a tight hydrogen-bond network is formed in the narrow space surrounding the γ-phosphate, two γ-phosphate sensors, and the backdoor residues (Fig. 2c). As described later, this narrow space is covered by the "phosphate tube" that provides the tunnel for the release of the inorganic phosphate.

These structures may represent the time course for the conformational change caused by ATP binding, namely, "isomerization", from KIF1A–AMPPCP to KIF1A–AMPPNP and finally to the KIF4–AMPPNP structure (Fig. 2a–c). KIF1A–AMPPCP represents the pre-isomerization state just after the collision between KIFs and ATP. KIF1A–AMPPNP represents the intermediate state during isomerization and KIF4–AMPPNP represents the pre-hydrolysis state, that is, the state just after isomerization and just before ATP hydrolysis. AMPPCP was reported to represent the collision ATP complex in myosins,[24] which is also adaptable to kinesins.[25] For the KIF1A–AMPPNP structure, one possible explanation of why the isomerization reaction stopped at the intermediate is the effect of the kinesin-3 conserved serine mutations in loop L11 (the corresponding residue in KIF4 is K250), as detailed later. This lysine residue in KIF4 plays a central role in facilitating the wound-up conformation of loop L11 in the KIF4 crystal structure, and thus, it is more difficult for KIF1A to adopt the wound-up conformation of L11 without this lysine residue.

Visualization of the time course for trapping the two waters in the nucleotide-binding pocket supports the two-water-mediated catalytic mechanism proposed for myosins and Eg5 (kinesin-5).[12,26] In the pre-isomerization state (KIF1A–AMPPCP), no water is trapped around the γ-phosphate of ATP. In the isomerization intermediate state (KIF1A–AMPPNP), one water is recruited to the phosphate tube by the conserved γ-phosphate-sensing residues (S211 and G244). In the pre-hydrolysis state (KIF4–AMPPNP), the other water is brought to the phosphate tube coupled with the closure of the backdoor. Before the hydrolysis of ATP, therefore, one water molecule interacts directly with the γ-phosphate, whereas the other connects the first water to the backdoor residues. In an analogous manner to myosin,[26] the first water becomes the lytic water that attacks the bound γ-phosphorus by bringing the proton to the second water. The second water is transiently converted into a hydronium ion (H_3O^+) whose proton will be further transferred to the backdoor E246. This two-water catalysis mechanism induces the hydrolysis of ATP, followed by release of the phosphate product through the phosphate tube.

Backdoor formation stabilizes the two switch regions

Backdoor closure also stabilizes two mobile loops, loop L9 (switch I) or loop L11 (switch II), which precede or follow the backdoor residues, respectively. In the KIF1A–AMPPNP structure, these two loops are flexible and invisible in the crystal structure (Fig. 1c and d). In the KIF4–AMPPNP structure, which possesses the totally closed backdoor, these two loops are stabilized and are clearly visible (Fig. 1b and c). The C-terminal half of the switch II L11 is wound up to form part of helix α4, thereby lengthening the N-terminal end of this helix by three turns. The N-terminal half of loop L11 is also wound up and forms a short helix behind helix α4 (Fig. 2f). Switch I loop L9 lies over these helices and covers the phosphate side of the nucleotide-binding pocket, making the tunnel or tube, namely, the phosphate tube, through which the γ-phosphate is released after the hydrolysis of ATP (Fig. 2d–f). The wall of this phosphate tube is composed of the switch I L9 (left and top) and the switch II α4–L11 (right and bottom) (Fig. 2e). In the phosphate tube, two waters are stabilized and the exit of the phosphate tube is the backdoor. From this point of view, in the previously reported KIF1A–ADP–vanadate structure, which represents the phosphate-release intermediate, the released phosphate located just outside of the backdoor has just passed through the phosphate tube.

Stabilization of these two flexible loops can be achieved as follows. The backdoor closure and the resulting water-mediated interactions stabilize the C-terminus of loop L9 and the N-terminus of loop L11 (Fig. 2c). Switch I L9 then adopts a pseudo-β-hairpin structure where five main-chain contacts between antiparallel L9 residues are observed and A205 positioned at the tip of this pseudo-β-hairpin interacts with T251 of L11, contributing to the stabilization of L9 and L11 (Fig. 2f). The interaction between R199

at the N-terminus of L9 and D241 at the N-terminus of L11, namely, the "Mg stabilizer", also contributes to this stabilization[10] (Fig. 2f). In addition to the interactions between the switch I and switch II loops, the linkages between these mobile loops and the rigid elements insensitive to ATP hydrolysis such as the P-loop, loop L7, or helix α6 are also necessary. From the front side of loop L11, the tri-residue interactions between R212 (L9), E260 (L11), and Y144 (L7), namely, the "latch", stabilize the wound-up conformation of helix α4[8] (Fig. 2f). Additionally, from the back side of L11, the hydrogen-bond network involving residues that include the "anchor" in the P-loop (Q89), loop L11 (K250), and helix α6 (N320 and E323) stabilizes the conformation of the N-terminal half of loop L11 (Fig. 2f).

Our structural result indicates that the backdoor closure stabilizes loop L11 by it being wound up into the long helix α4, and this mechanism might be common at least between N-kinesins. As such, KIFs exhibit a shorter helix α4 in the nucleotide-free state and ATP binding stabilizes loop L11 to give the longest helix α4, information that is further relayed to the neck linker. This structural model fits very well with the previous structural report of the kar3–microtubule complex[14] that indicates the shortest helix α4 in the nucleotide-free state, and a similar structure was also reported with KIF1A.[8] It is, however, apparently inconsistent with the previous report that showed KIF5 on the microtubule giving a long helix α4 throughout all the nucleotide states.[15] One possible solution is that this discrepancy might come from the difference between N-kinesin and C-kinesin, or from the class-specific difference. Further high-resolution structural studies of KIFs complexed with tubulin or microtubules are awaited to solve this discrepancy.

Backdoor formation induces full docking of the neck linker through a conformational change to switch II

Backdoor formation further affects the conformation of L11–α4–L12–α5–L13 in switch II. Stabilization of loop L11, which is located close to the catalytic center (left side when on the microtubule), induces the clockwise rotation of helices α4 and α5 up to 5° during the isomerization step (Fig. 3a–c). This rotation relays the conformational change to loop L13 located on the other side of the catalytic core (right side when on the microtubule), which provides the stable docking site for the neck linker, resulting in the full docking of the neck linker to the catalytic core. In all three structures with ATP analogs, the interaction between the neck initial segment and helix α4 through the conserved hydrophobic interaction between I337 (neck initial segment) and L278 (α4), which is required for the

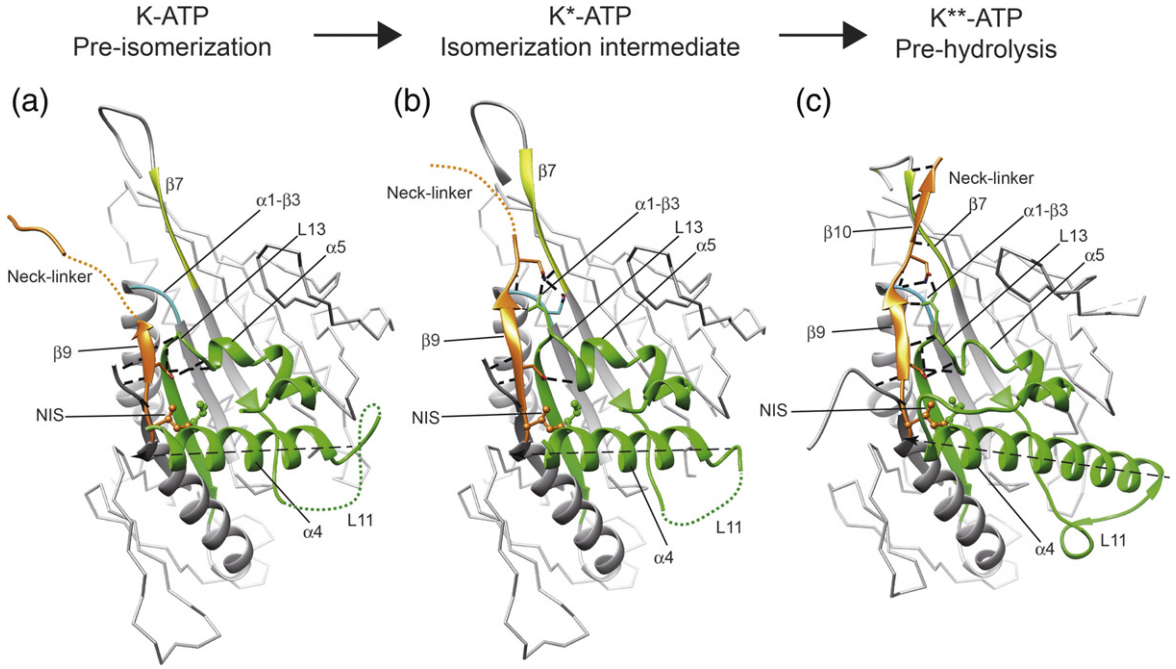

Fig. 3. Sequential docking of the neck linker induced by ATP binding (isomerization). (a) Pre-isomerization state with KIF1A–AMPPCP. (b) Isomerization intermediate state with KIF1A–AMPPNP. (c) Pre-hydrolysis state with KIF4–AMPPNP. Bold broken lines indicate the interactions between the neck linker and the catalytic core. The dashed arrow indicates the helical axis of helix α4, showing the clockwise rotation during the isomerization reaction.

release of ADP, is observed (Fig. 3a–c).[8] During the isomerization step from the pre-isomerization state to the isomerization intermediate state, the next segment of the neck linker forms β9 with loop L13 (Fig. 3a and b). The remaining segment further forms β10 with α1–β3 and β7 after the isomerization step (Fig. 3c). The sequential docking of β9 and β10 is, therefore, observed from the pre-isomerization state (KIF1A–AMPPCP), to the isomerization intermediate (KIF1A–AMPPNP), to the pre-hydrolysis state (KIF4–AMPPNP), indicating that the isomerization reaction from the nucleotide-binding pocket tightly regulates the docking of the neck linker to the core. Considering that the neck linker connects two motor heads in the dimeric KIFs and that its length is optimized to be strained if both heads are bound to the microtubule, this tight regulation of the neck-linker conformation by ATP binding to the catalytic center of the rigor head serves as the structural basis for placing the tethered head to the next binding site. This results in the power stroke in the asymmetric hand-over-hand motility by achieving the tight coupling of the ATPase cycle between two motor heads necessary for the processive movement of dimeric kinesins (ATP gating).[7,8]

Microtubule-binding interface of the KIF4 motor domain

To determine the interactions between KIF4 and the microtubule, in silico docking of the high-resolution crystal structure of KIF4 into a medium-resolution cryo-EM map of the KIF4–microtubule would be informative. Currently, however, there is no available cryo-EM structure reported for the KIF4–microtubule complex. Hence, we docked the atomic structure of KIF4–AMPPNP into the cryo-EM structure of the KIF1A (AMPPNP)–microtubule complex,[13] because the tertiary structure of KIF4–AMPPNP is very similar to the KIF1A–AMPPNP structure, except for two switch regions as described above.

Owing to the similarity between the KIF4 and KIF1A motor domains, the atomic structure of KIF4 fitted very well with the cryo-EM structure of the KIF1A–microtubule complex (Fig. 4a). We then checked the details of the fitting of the two switch regions where the largest differences were observed between the crystal structures of KIF4 and KIF1A. As described above, the crystal structure of KIF1A with AMPPNP gives a short helix α4. The cryo-EM structure of the KIF1A (AMPPNP)–microtubule complex, however, has a longer tubular density at the corresponding region (red dotted circle), such that residual density remains to the left side of helix α4 (Fig. 4b). Surprisingly, when KIF4–AMPPNP is fitted into the cryo-EM density of the KIF1A–microtubule complex, the length of helix α4 of KIF4 fits nicely into this long tubular density in the KIF1A–microtubule density (Fig. 4c). In contrast, the N-terminal half of loop L11 that makes the short one-turn helix in the crystal structure of KIF4 does not fit well into the cryo-EM density of the KIF1A–microtubule complex (Fig. 4d). Thus, we performed in silico docking of the KIF4 structure into the previously solved cryo-EM structure of KIF5 (AMPPNP)–microtubule to examine whether this difference is derived from the structural differences between apo-KIFs and KIFs bound to the microtubule, or simply from a family-specific difference (between kinesin-3 and kinesin-4).[15] The KIF4 crystal structure was found to fit perfectly into the cryo-EM density of the KIF5–microtubule complex (Fig. 4e). The helical conformation of L11 and the long helix α4 of KIF4 fit into the cryo-EM density of the KIF5–microtubule very well. Furthermore, the conformation of the switch I loop L9 also fits perfectly to this map. This perfect fitting further confirms that the crystal structure of KIF4 with AMPPNP represents a true pre-hydrolysis state that may be a common structure for most N-kinesins.

In the crystal structure, the wound-up conformation of loop L11 is supported by the L11–α6–P-loop interactions (anchor) through K250 of L11. The conformation of L9 is further supported by the wound-up conformation of L11, as described above. From the sequence alignment of the N-terminal kinesin motors, K250 is mutated to serine only in the kinesin-3 family of motors (Fig. 4f). This mutation explains why L11 of KIF4 does not fit well into the cryo-EM density of the KIF1A–microtubule complex. It also explains why KIF1A–AMPPNP in the crystal structure could not adopt the wound-up conformation of L11, as discussed above. This difference may affect some KIF1A-specific features such as strong binding with microtubules or the non-selective strong binding of KIF1A to both GTP and GDP microtubules in the axon and dendrite.[27]

KIF4-specific sequences on the microtubule-binding surface

We have previously discussed the general structural features of the N-kinesins. In this final section, we will discuss the structural implications for the KIF4-specific regulation of microtubule dynamics, because this is the first report of the atomic structure of KIF4. KIF4 was reported to contribute to mitotic spindle organization and chromosome positioning[28,29] by maintaining the correct size of overlapped spindle microtubules through inhibition of their elongation,[30] although the mechanism through which KIF4 regulates microtubule dynamics remains unclear. From the sequence alignment of the N-kinesins, KIF4 has the standard motor domain of the N-kinesins in which important regions for ATP catalysis and microtubule-based motility, including the P-loop, the two switch regions, and the neck linker, are highly conserved. Consistently, ATPase activity of the KIF4 motor domain was reported to be activated by microtubule

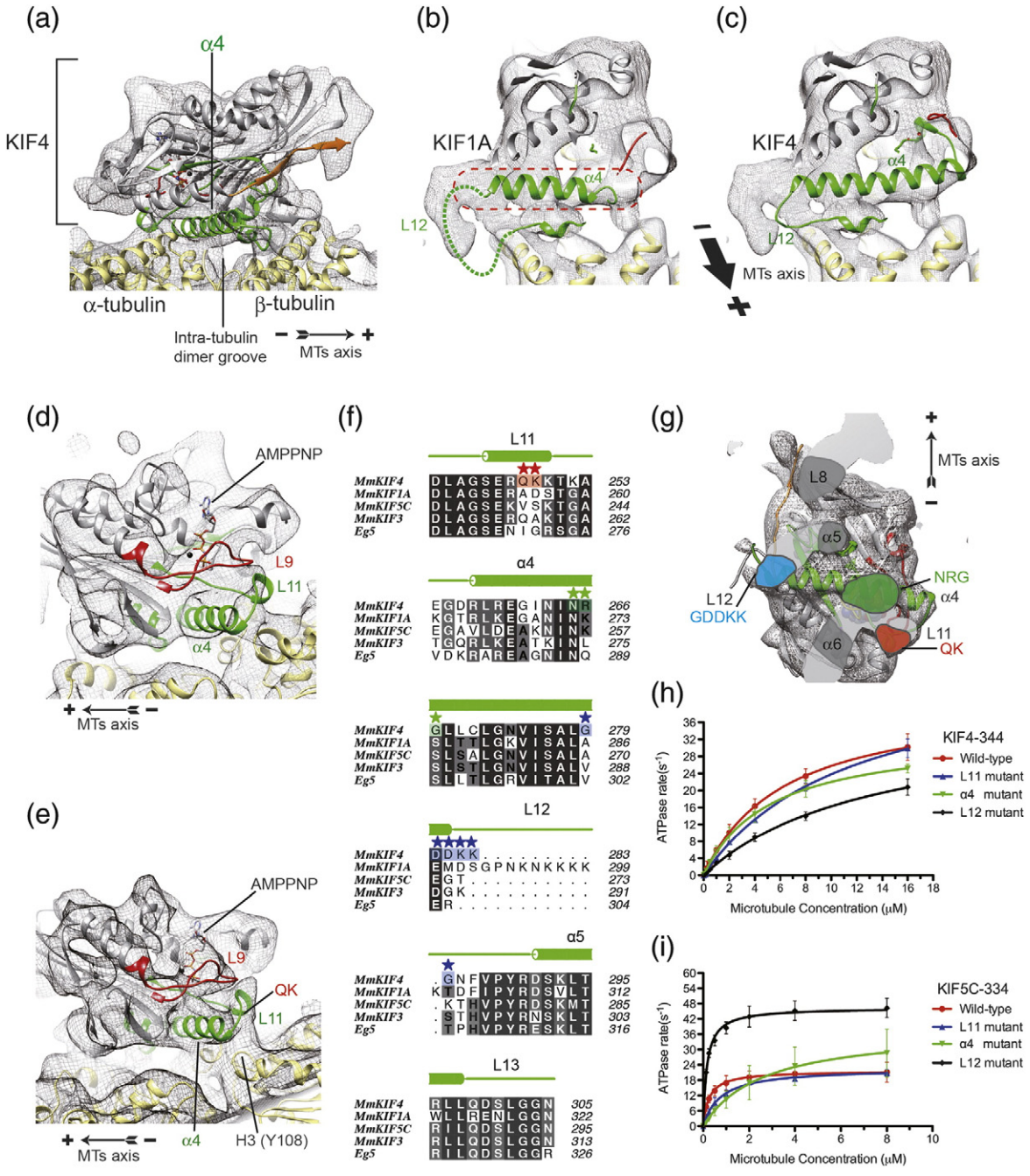

Fig. 4. Expected microtubule-binding surface of the KIF4 motor domain. (a) Crystal structure of KIF4–AMPPNP docked into the cryo-EM map of the KIF1A–microtubule complex as seen from the right side of the microtubule protofilament. (b) Crystal structure of KIF1A–AMPPNP docked into the cryo-EM map of the KIF1A–microtubule complex as seen from the plus end of the microtubule. The red dashed circle indicates the long tubular density corresponding to helix α4. (c) Crystal structure of KIF4–AMPPNP docked into the cryo-EM map of the KIF1A–microtubule complex as seen from the plus end of the microtubule. (d) Crystal structure of KIF4–AMPPNP docked into the cryo-EM map of the KIF1A–microtubule complex as seen from the left side of the microtubule protofilament. (e) Crystal structure of KIF4–AMPPNP docked into the cryo-EM map of the KIF5–microtubule complex as seen from the left side of the microtubule protofilament. (f) Sequence alignment of the switch II regions of the N-kinesins. (g) Putative microtubule-binding site of the KIF4 motor domain seen from the microtubule-binding side with the plus end to the top. (h) ATPase activities of wild-type KIF4 and three KIF4 mutants. (i) ATPase activities of wild-type KIF5C and three KIF5C mutants. Error bars represent the SD of at least three independent measurements. Microtubule-dependent ATPase activity was measured using the EnzChek® Phosphate Assay Kit (Molecular Probes) and a V-630 Bio spectrophotometer (JASCO), as described previously.[8]

binding, and the anterograde motility of KIF4 along the microtubule was also reported.[31] Unlike other N-kinesins, however, the motor domain of KIF4 regulates microtubule dynamics through direct inhibition of microtubule elongation and contraction.[32] Like kinesin-8 motors,[33] the *Xenopus laevis* KIF4 Xklp1 motor can bind both the microtubule and the free tubulin dimer, which also stimulates the ATPase activity of KIF4.[32] Hence, the motor domain of KIF4 functions to regulate microtubule dynamics as well as the standard motor function of N-kinesins.

Differences in the microtubule-binding interface between KIF4 and other N-kinesins should be initially considered to determine the specificity of KIF4 for the microtubule. From the pseudo atomic model of the KIF4–microtubule, the expected contact surface of KIF4 to the microtubule is composed of the following five regions: loop L8, loop L11, helix α4, loop L12, and helix α6 (Fig. 4g). Of these regions, contacts through helix α4, the preceding loop L11, and the following loop L12 play central roles in controlling the ATPase-dependent microtubule binding to produce motility along the microtubule.[8–10,13] In this area, three KIF4-specific amino acid modifications are concentrated. The binding site mediated by loop L11 is located at the left side of the α-tubulin (H3′ helix) and slightly toward the rear (minus end) side from the intra-tubulin dimer groove, where the KIF4-specific Q248 and K249 form possible hydrogen bonds with Y108 of helix H3′ of α-tubulin (Fig. 4e and g). Around the center line of the microtubule protofilament, the helix-α4-mediated microtubule-binding site is located and fitted into the intra-tubulin dimer groove. Although the main contact with this binding site is mediated by the conserved N273–R274 residues, the next amino acid, G275, is specific to KIF4. At the right side of the β-tubulin in the same tubulin dimer and slightly toward the front side (plus end) from the intra-tubulin dimer groove, loop L12 binds to the C-terminal half of helix H12 or the following E-hook (C-terminal tail of tubulin). KIF4 has the specific L12 sequence, GDDKKG, and the conformation of L12 in KIF4 does not fit well to either the KIF1A or KIF5 microtubule complexes (Fig. 4c). Hence, the binding of KIF4 to the microtubule may affect the interaction within the tubulin dimer by increasing or decreasing the curvature of the intra-tubulin dimer interface with some twist. A previous report suggested that the longitudinal interface of tubulins including intra- and inter-dimer contacts significantly affects the stability of the microtubule.[34] Therefore, these three regions are possible contributors to the KIF4-specific stabilization of microtubule dynamics.

To test the importance of these unique sequences at the microtubule-binding surface for the KIF4-specific function, we introduced several mutations into these three regions and examined the steady-state kinetics of the microtubule-stimulated ATPase. The basic strategy for introducing the mutations was to mutually exchange the corresponding sequences between KIF4 and KIF5C to make chimeric constructs of KIF4 and KIF5C. QK in loop L11 of KIF4 was exchanged with VS of KIF5C (red star in Fig. 4f). G in helix α4 of KIF4 was exchanged with S of KIF5C (green star in Fig. 4f). GDDKKG in loop L12 of KIF4 was exchanged with AEGTK of KIF5C (blue star in Fig. 4f).

We first examined the microtubule-stimulated ATPase of wild-type monomeric KIF4 (1–344) and monomeric KIF5C (1–334) (Fig. 4h and i). The turnover rate of the KIF4 ATPase was comparable with that of KIF5C and other typical kinesins [k_{cat} (KIF4) = 42.1 ± 2.29 s^{-1}; k_{cat} (KIF5) = 21.7 ± 0.857 s^{-1}]. The Michaelis–Menten constant ($K_{M, MT}$) was, however, 1 order of magnitude higher than that of KIF5C or other typical kinesins [$K_{M, MT}$ (KIF4) = 6.34 ± 0.770 μM; $K_{M, MT}$ (KIF5C) = 0.260 ± 0.0457 μM], indicating the weak binding of KIF4 to the microtubule. This feature was also reported for *X. laevis* KIF4 Xklp1,[32] although mammalian KIF4 seems to show a milder phenotype than amphibian KIF4. In fact, unlike the previous report on Xklp1, the tubulin dimer was not observed to activate the KIF4 ATPase in the mouse monomeric KIF4 construct (data not shown).

Then, the steady-state ATPase activities of three types of chimeric construct were examined. Although the mutations in loop L11 did not show a marked effect on the steady-state ATPase, the mutations in loop L12 and helix α4 significantly affected the ATPase in a completely different manner (Fig. 4h and i). The KIF4-specific sequence, GDDKKG in L12, increased the ATPase turnover rate (k_{cat} = 46.4 ± 0.936 s^{-1}), while it decreased the Michaelis–Menten constant ($K_{M, MT}$ = 0.164 ± 0.0171 μM). The substrate specificity for this interaction ($k_{cat}/K_{M, MT}$), which is thought to be dependent solely on rate constants involved in microtubule binding, showed a more than threefold increase in comparison to the wild-type KIF5C [$k_{cat}/K_{M, MT}$ (wild-type KIF5C) = 83.4 s^{-1} $μM^{-1}$; $k_{cat}/K_{M, MT}$ (KIF5C L12 mutant) = 282 s^{-1} $μM^{-1}$]. Conversely, the KIF4 mutant with loop L12 of KIF5C (AEGTK) showed an approximately threefold lower substrate specificity in comparison to the wild-type KIF4 [$k_{cat}/K_{M, MT}$ (wild-type KIF4) = 6.64 s^{-1} $μM^{-1}$; $k_{cat}/K_{M, MT}$ (KIF4 L12 mutant) = 2.89 s^{-1} $μM^{-1}$]. Considering that loop L12 contributes mainly to the weak-binding state (ADP state),[4] some aspect of microtubule binding in the weak-binding state has been altered with the L12 mutation and this tuning will be required for KIF4, which exhibits native weak binding to the microtubule. In contrast, a single amino acid mutation (G ⇔ S) in helix α4 had a completely different effect on the kinesin ATPase (Fig. 4h and i). KIF4 with G267S slightly decreased both the turnover rate and the Michaelis–Menten constant with an almost equivalent specificity constant to that of wild-type KIF4. KIF5C with S258G, however, exhibited an

increased Michaelis–Menten constant of 1 order of magnitude greater than the wild type. Therefore, the S258G mutant of KIF5C apparently showed a similar ATPase curve to the wild-type KIF4. Because this serine is not expected to be included in the main microtubule-binding surface throughout all nucleotide states, this glycine mutation may indirectly affect microtubule binding through a unique strategy such as the destabilization of helix α4 at some point during the ATPase cycle. In either case, the kinetic data collectively suggest that at least two KIF4-specific sequences in helix α4 and loop L12 must be necessary for KIF4-specific functions, and further structural studies of the KIF4–microtubule complex as well as biochemical and biophysical studies are needed to determine the full molecular mechanism by which KIF4 inhibits microtubule dynamics.

Accession numbers

Coordinates and structure factors have been deposited in the Protein Data Bank with accession numbers 3ZFC (NW12A) and 3ZFD (41XU).

Acknowledgements

We thank H. Fukuda, H. Sato, and T. Akamatsu for assistance, and other members of the Hirokawa laboratory for discussions. This work was supported by a Center of Excellence Grant-in-Aid from the Ministry of Education, Culture, Sports, Science and Technology of Japan to N.H.

Supplementary Data

Supplementary data to this article can be found online at http://dx.doi.org/10.1016/j.jmb.2013.03.004

Received 12 December 2012;
Received in revised form 28 February 2013;
Accepted 2 March 2013
Available online 7 March 2013

Keywords:
x-ray crystallography;
molecular motor;
kinesin;
ATPase;
microtubule

Abbreviations used:
KIF, kinesin superfamily protein; AMPPCP, β,γ-methyleneadenosine 5-triphosphate; AMPPNP, adenylyl imidodiphosphate; cryo-EM, cryo-electron microscopy.

References

1. Hirokawa, N., Noda, Y., Tanaka, Y. & Niwa, S. (2009). Kinesin superfamily motor proteins and intracellular transport. *Nat. Rev. Mol. Cell Biol*, **10**, 682–696.
2. Hirokawa, N., Nitta, R. & Okada, Y. (2009). The mechanisms of kinesin motor motility: lessons from the monomeric motor KIF1A. *Nat. Rev. Mol. Cell Biol*, **10**, 877–884.
3. Nitta, R. & Hirokawa, N. (2013). In *Fundamental Properties and Structure of Kinesin. Encyclopedia of Biophysics* (Roberts, G. C. K., ed.), 1, Springer-Verlag, Berlin Heidelberg.
4. Asbury, C. L., Fehr, A. N. & Block, S. M. (2003). Kinesin moves by an asymmetric hand-over-hand mechanism. *Science*, **302**, 2130–2134.
5. Yildiz, A., Tomishige, M., Vale, R. D. & Selvin, P. R. (2004). Kinesin walks hand-over-hand. *Science*, **303**, 676–678.
6. Rice, S., Lin, A. W., Safer, D., Hart, C. L., Naber, N., Carragher, B. O. *et al.* (1999). A structural change in the kinesin motor protein that drives motility. *Nature*, **402**, 778–784.
7. Alonso, M. C., Drummond, D. R., Kain, S., Hoeng, J., Amos, L. & Cross, R. A. (2007). An ATP gate controls tubulin binding by the tethered head of kinesin-1. *Science*, **316**, 120–123.
8. Nitta, R., Okada, Y. & Hirokawa, N. (2008). Structural model for strain-dependent microtubule activation of Mg-ADP release from kinesin. *Nat. Struct. Mol. Biol.* **15**, 1067–1075.
9. Kikkawa, M., Sablin, E. P., Okada, Y., Yajima, H., Fletterick, R. J. & Hirokawa, N. (2001). Switch-based mechanism of kinesin motors. *Nature*, **411**, 439–445.
10. Nitta, R., Kikkawa, M., Okada, Y. & Hirokawa, N. (2004). KIF1A alternately uses two loops to bind microtubules. *Science*, **305**, 678–683.
11. Cochran, J. C., Sindelar, C. V., Mulko, N. K., Collins, K. A., Kong, S. E., Hawley, R. S. & Kull, F. J. (2009). ATPase cycle of the nonmotile kinesin NOD allows microtubule end tracking and drives chromosome movement. *Cell*, **136**, 110–122.
12. Parke, C. L., Wojcik, E. J., Kim, S. & Worthylake, D. K. (2010). ATP hydrolysis in Eg5 kinesin involves a catalytic two-water mechanism. *J. Biol. Chem.* **285**, 5859–5867.
13. Kikkawa, M. & Hirokawa, N. (2006). High-resolution cryo-EM maps show the nucleotide binding pocket of KIF1A in open and closed conformations. *EMBO J.* **25**, 4187–4194.
14. Hirose, K., Akimaru, E., Akiba, T., Endow, S. A. & Amos, L. A. (2006). Large conformational changes in a kinesin motor catalyzed by interaction with microtubules. *Mol. Cell*, **23**, 913–923.
15. Sindelar, C. V. & Downing, K. H. (2010). An atomic-level mechanism for activation of the kinesin molecular motors. *Proc. Natl Acad. Sci. USA*, **107**, 4111–4116.
16. Kabsch, W. (2010). Xds. *Acta Crystallogr., Sect. D: Biol. Crystallogr.* **66**, 125–132.
17. Evans, P. R. (2011). An introduction to data reduction: space-group determination, scaling and intensity statistics. *Acta Crystallogr., Sect. D: Biol. Crystallogr.* **67**, 282–292.

18. Vagin, A. & Teplyakov, A. (2010). Molecular replacement with MOLREP. *Acta Crystallogr., Sect. D: Biol. Crystallogr.* **66**, 22–25.
19. Murshudov, G. N., Skubak, P., Lebedev, A. A., Pannu, N. S., Steiner, R. A., Nicholls, R. A. *et al.* (2011). REFMAC5 for the refinement of macromolecular crystal structures. *Acta Crystallogr., Sect. D: Biol. Crystallogr.* **67**, 355–367.
20. Emsley, P., Lohkamp, B., Scott, W. G. & Cowtan, K. (2010). Features and development of Coot. *Acta Crystallogr., Sect. D: Biol. Crystallogr.* **66**, 486–501.
21. Sprang, S. R. (1997). G protein mechanisms: insights from structural analysis. *Annu. Rev. Biochem.* **66**, 639–678.
22. Vale, R. D. (2003). The molecular motor toolbox for intracellular transport. *Cell*, **112**, 467–480.
23. Geeves, M. A. & Holmes, K. C. (1999). Structural mechanism of muscle contraction. *Annu. Rev. Biochem.* **68**, 687–728.
24. Koretz, J. F. & Taylor, E. W. (1975). Transient state kinetic studies of proton liberation by myosin and subfragment 1. *J. Biol. Chem.* **250**, 6344–6350.
25. Kull, F. J. & Endow, S. A. (2002). Kinesin: switch I & II and the motor mechanism. *J. Cell. Sci.* **115**, 15–23.
26. Onishi, H., Mochizuki, N. & Morales, M. F. (2004). On the myosin catalysis of ATP hydrolysis. *Biochemistry*, **43**, 3757–3763.
27. Nakata, T., Niwa, S., Okada, Y., Perez, F. & Hirokawa, N. (2011). Preferential binding of a kinesin-1 motor to GTP-tubulin-rich microtubules underlies polarized vesicle transport. *J. Cell. Biol.* **194**, 245–255.
28. Vernos, I., Raats, J., Hirano, T., Heasman, J., Karsenti, E. & Wylie, C. (1995). Xklp1, a chromosomal *Xenopus* kinesin-like protein essential for spindle organization and chromosome positioning. *Cell*, **81**, 117–127.
29. Wandke, C., Barisic, M., Sigl, R., Rauch, V., Wolf, F., Amaro, A. C. *et al.* (2012). Human chromokinesins promote chromosome congression and spindle microtubule dynamics during mitosis. *J. Cell. Biol.* **198**, 847–863.
30. Bieling, P., Telley, I. A. & Surrey, T. (2010). A minimal midzone protein module controls formation and length of antiparallel microtubule overlaps. *Cell*, **142**, 420–432.
31. Sekine, Y., Okada, Y., Noda, Y., Kondo, S., Aizawa, H., Takemura, R. & Hirokawa, N. (1994). A novel microtubule-based motor protein (KIF4) for organelle transports, whose expression is regulated developmentally. *J. Cell. Biol.* **127**, 187–201.
32. Bringmann, H., Skiniotis, G., Spilker, A., Kandels-Lewis, S., Vernos, I. & Surrey, T. (2004). A kinesin-like motor inhibits microtubule dynamic instability. *Science*, **303**, 1519–1522.
33. Gupta, M. L., Jr., Carvalho, P., Roof, D. M. & Pellman, D. (2006). Plus end-specific depolymerase activity of Kip3, a kinesin-8 protein, explains its role in positioning the yeast mitotic spindle. *Nat. Cell. Biol.* **8**, 913–923.
34. Wang, H. W. & Nogales, E. (2005). Nucleotide-dependent bending flexibility of tubulin regulates microtubule assembly. *Nature*, **435**, 911–915.